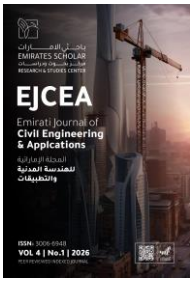

Emirati Journal of Civil Engineering and Applications
Vol 4 Issue 1 (2026)
Pages (101 -117)

Available at
www.emiratesscholar.com

Optimization of Reinforced Concrete Deep Beams Using Data-Driven Parametric Performance Indicators

Tufail Mabood
Civil Engineer at UET Peshawar, University of Engineering and Technology, Peshawar, Pakistan
*Corresponding author: 13bnciv0557@uetpeshawar.edu.pk

ARTICLE HISTORY

Received: 20 Fep 2026.
Accepted: 17 Mar 2026.
Published: 19 Jun 2026.

PEER - REVIEW STATEMENT:

This article was reviewed under a double-blind process by independent reviewers.

HOW TO CITE

Mabood, T. (2026). Optimization of Reinforced Concrete Deep Beams Using Data-Driven Parametric Performance Indicators. Emirati Journal of Civil Engineering and Applications, 4(1),101-117. https://doi.org/10.54878/xqyna996

ABSTRACT

The present study proposes a multi-objective optimization model for reinforced concrete deep beams based on the study and improvement of structural performance using multi objective optimization. In traditional design methodologies, the complex relationships between various parameters are generally ignored. The present study was based on the formulation of four objectives: F_1 (Cross-sectional Efficiency), F_2 (Reinforcement Contribution Ratio), F_3 (Tensile Mechanism), and F_4 (Structural Gradient). The objectives F_1, F_2, F_3, and F_4 were combined with various parameters and material characteristics to obtain optimal design findings. F_1 and F_4 are related to efficient cross-sectional design and uniform stress. F_2 and F_3 are related to tensile and compressive effects of vertical and horizontal bars. The conclusions revealed efficient design and proportions of reinforced materials for capacities to bear loads and minimal use of materials. The importance of multi-objective optimization is emphasized in the discussion, which states that it gives a more precise view of structural behavior than the conventional single-parameter design. In general, the paper has established a generalized design approach for reinforced concrete deep beams that incorporate efficiency, safety, and practicability. The results of this research provide valuable information for engineers and pave the way for further experimental verification and parametric studies.

Keywords: *Reinforced concrete deep beam, multi-objective optimization, structural efficiency, reinforcement configuration, material optimization*

Introduction

Analysis and design of the structural behavior of reinforced concrete deep beams have been considered a major turning point from classical Bernoulli-Euler bending theory applicable to slender members only. Characterized by a shear span depth ratio (a/d) typically less than 2.0, deep beams have been treated as Discontinuity regions (D-regions), where the strain distribution is not linear from a physical standpoint [1], [2]. Within these elements, the internal transfer is defined through an arching action, enabling a direct diagonal compression field or a concrete strut to occur from the load point to the support. This mechanism necessitates the adoption of a design philosophy which treats the design as a discrete system of paths of internal forces rather than a homogeneous flexural system [3], [4].

The evolution of the design of deep beams, like other aspects of beam design, has been towards rational rather than formula-based code provisions. Early experimental work showed that the shear capacity of beams is significantly higher for a beam of deeper section. This is because of the efficiency of the diagonal compression strut [5]. The problem, however, is that this higher capacity is often accompanied by a lack of ductility, and deep beam failures are invariably sudden and catastrophic, characterized by diagonal tension cracking, longitudinal splitting, and explosive crushing in the nodal zones [6]. These observations led to the formulation of the Strut-and-Tie Model, which conceptually represents the deep beam as a truss, where the concrete is treated as compressed members or struts, and the steel reinforcement is treated as the members that carry the tensile forces. In spite of the efficacy of the Strut-and-Tie Model, the implementation of the model is an extremely complex process, as it calls for the pre-definition of the truss and the calculation of the efficiency factors of the bottle-shaped members that bulge and crack due to the high levels of stress [7], [8]

Experimental databases have additionally helped to reinforce the significance of the size effect as an integral factor affecting deep beam behavior. It has been found that, as the absolute depth of a beam increases, its nominal shear strength typically reduces, even for constant proportion [9], [10]. This has been largely attributed to the increase in width of diagonal cracking, which diminishes the performance of secondary but vital mechanisms of shear transfer, namely aggregate interlock [11]. Moreover, the utilization of High-Strength Concrete (HSC) in deep beam constructions has revealed some complicating factors. Indeed, the high strengths of HSC can be offset by the reduced ductility which can lead to splitting or crushing of concrete struts under decreased strain values for HSC compared to normal strength concrete structures [12]. This has again emphasized the importance of "intelligent" reinforcement detailing, which may involve the placement of higher levels of horizontal and vertical reinforcement, where possible, to act to control the concrete, and hence the internal compression field [13], [14], [15].

The effectiveness debate surrounding vertical and horizontal web reinforcement has continued to be at the core of deep beam literature evolution. For slender beams, vertical stirrups remain dominant, but for particularly deep beams that possess high vertically oriented struts, horizontal "skin" reinforcement may be just as effective, if not more so [16], [17]. This horizontal reinforcement has been found to counter transverse tensile stresses that equally divert from the formation of a bulge within the diagonal strut located between the load and support members. Without this horizontal reinforcement, splitting and destabilization of these struts are possible, eliminating any arcing effects from taking place entirely. This has been a turning point within details and

topologies, providing much-needed support to computational optimization techniques that utilize precise location and placement to match reinforcement where required according to inherent stresses [18].

Initially, optimization problems in deep beams were concerned with single-objective problems, mainly minimizing the cost of materials or the total volume of steel used [19], [20]. However, these problems were often found to produce structures that were impracticable in terms of constructability. They could also emerge with worsened serviceability as exemplified by excessive cracks under service loads [21], [22], [23]. The advent of topology optimization, on one hand, provided an avenue for auto-mating the determination of efficient paths through which structures could respond to external forces. However, there was a high probability that the achieved "organic" forms were impracticable and unrealistic in terms of constructability [24]. This necessitated the development of a framework that could handle a variety of optimization problems, commonly referred to as a multi-objective optimization framework.

This study presents a data-driven, rotational multi-objective optimization (MOO) framework that concurrently maximizes geometric efficiency (F_1), reinforcement balance (F_2), tensile engagement (F_3), and global performance (F_4) to identify a Pareto front of mechanically sound, experimentally validated deep-beam configurations, thereby shifting the design paradigm toward a "form-follows-flow" approach that balances strength, serviceability, and economy.

Research Gap

Despite the extensive documentation of reinforced concrete deep beam performance, a significant research gap exists in the lack of high-dimensional, multi-objective optimization frameworks capable of simultaneously addressing the non-linear interactions between thirteen material and geometric variables, reinforcement participation ratios, and structural gradients, a limitation that often results in designs that are either overly conservative or structurally inefficient due to the static and single-objective nature of current design methodologies.

Method

The computational framework, as shown schematically in Figure 1, effectively incorporates a given empirical deep beam data set by following a three-stage process consisting of data normalization, parametric search, and multi-objective evaluation. Experimental data is mapped to a given bounded evolutionary search domain, with four discrete fitness functions being utilized to determine structural performance according to a given unit system (mm, kN, MPa), to maintain dimensional homogeneity. The Octopus MOO Optimizer is used to reduce the competitive effects underlying structural performance according to a stabilized Pareto front, with post-processing being carried out using a Python script to refine results according to trendline regression.

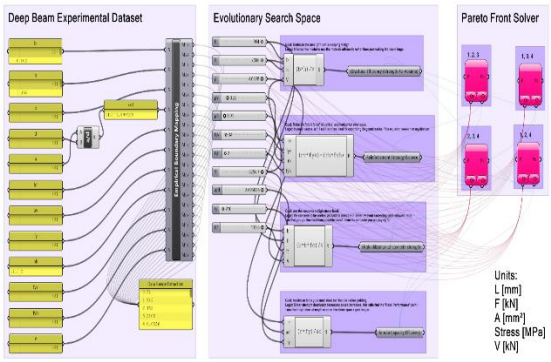

Figure 1: Integrated structural optimization workflow mapping empirical deep beam datasets to a multi-objective Pareto front solver via evolutionary parametric modeling.

Experimental Data as the Basis of the Model

A database of experimental RC deep beams was created from the literature. For each test specimen, the set of parameters (in Equation

(2)) were extracted. These data were introduced into Grasshopper panels to determine the admissible limits of each variable. These values were entered into Grasshopper panels to calculate the admissible limits of each parameter. For every variable x_i, the bounds were defined as in Equation (1).

$$x_i \in [x_i^{min}, x_i^{max}] \quad (1)$$

The obtained limits were then used to set the values of the sliders that controlled the Octopus genomes, ensuring that the parametric exploration and optimization stayed within the experimentally observed and physically validated domain.

3.2 Decision Vector and Feasible Domain

The deep-beam configuration is described by a decision vector, x, which combines the fundamental geometric, material, reinforcement, and loading parameters into a unified mathematical construct. Each distinct beam configuration is represented by a discrete point in the high-dimensional parameter space, which can be explored systematically as expressed in Equation (2):

$$x = [h, b, d, a, \frac{a}{d}, f_c', \rho, f_y, \rho_v, f_{yv}, \rho_h, f_{yh}, V]^T \in R^{13} \quad (2)$$

where h, d, b, a are in millimeters (mm), $(\frac{a}{d})$ is dimensionless, $f_c', f_y, f_{yv}, f_{yh}$ are in megapascals (MPa), ρ, ρ_v, ρ_h are ratios (dimensionless), and V is in kilonewtons (kN). The feasible search region for this vector is specified as a bounded area in grasshopper scroll bars, obtained from the experimental database. The boundaries of this area are not presumed but obtained directly from test results, which are as per the Equation (3).

$$x \in \Omega = \{ x \mid \begin{bmatrix} h \\ b \\ d \\ a \\ (a/d) \\ f_c' \\ \rho \\ f_y \\ \rho_v \\ f_{yv} \\ \rho_h \\ f_{yh} \\ V \end{bmatrix} = \begin{bmatrix} 152 \\ 137 \\ 51 \\ 80 \\ 0.2 \\ 11.3 \\ 0.0026 \\ 210 \\ 0 \\ 0 \\ 0 \\ 0 \\ 20.7 \end{bmatrix}^T + \xi . \left(\begin{bmatrix} 2100 \\ 2000 \\ 914 \\ 4375 \\ 2.7 \\ 120.1 \\ 4.08 \\ 1330 \\ 2.45 \\ 1051 \\ 2.45 \\ 855 \\ 6294 \end{bmatrix}^T - \begin{bmatrix} 152 \\ 137 \\ 51 \\ 80 \\ 0.2 \\ 11.3 \\ 0.0026 \\ 210 \\ 0 \\ 0 \\ 0 \\ 0 \\ 20.7 \end{bmatrix}^T \right), \xi \in [0,1]^{13} \} \quad (3)$$

In this formulation, each element of the normalized vector ξ is transformed element-wise by multiplication into the physical space, yielding a candidate vector, x, that meets all the experimental constraints.

3.3 Formulation of Structural Performance Objectives

Equation (4) represents the multi-objective optimization problem on the feasible domain Ω (as presented in Equation (3)). In order to analyze deep beam performance under a unified mathematical formulation, a multi-objective optimization method is employed. This approach further facilitates the simultaneous evaluation of several characteristics, as opposed to using single performance indicators. Furthermore, all possible solutions are restricted by considering the experimentally feasible domain Ω (Equation (3)), ensuring the physical results at all stages of optimization. The optimization problem is defined as the maximization of several performing indicators for all possible decision vectors, while considering the experimentally feasible domain

Ω (Equation (3).

These performing indicators defined are different mechanical characteristics in shear behavior.

$$\max_{x \in \Omega} F(x) = \max_{x \in \Omega} \{F_1, F_2, F_3, F_4\} \quad (4)$$

Equation (5) accounts for the geometric efficiency of the section in relation to the applied shear force. In this context, geometric efficiency is related to the gross sectional area of the structural member ($A_g = b.h$), as well as the shear capacity (V). When the value of F_1 is higher, it implies that the geometric reserve is also higher, meaning that the level of stress concentration on the structure is much lower, thus increasing the level of structural stability with respect to external forces. In addition to addressing efficiency, Equation (5) is a basic geometric parameter related to the overall optimization procedure, as presented in Equation (7) and Equation (8). The isolation of the area-to-load ratio in this index provides a reference value for the structural efficiency that is not dependent on any particular material properties or reinforcement layout.

$$F_1(x) = \frac{A_g}{V} = \frac{b.h}{V}, x \in \Omega \quad (5)$$

Equation (6) calculates the dominance of vertical shear reinforcement, taking into consideration the effect of horizontal reinforcement. The F_2 is solely based on the interaction between vertical and horizontal shear reinforcement. It determines the effect of vertical reinforcement effectiveness in the presence of horizontal reinforcement in the web. By multiplying the reinforcement ratios with their respective yield strengths, the F_2 determines the dominance of vertical steel after considering the effects of transverse reinforcement. This index quantifies the internal balance between the two directions of reinforcement, which are responsible for resisting diagonal cracking and shear transfer. Unlike the F_1, F_2 isolates steel and its interaction, providing information on the effect of steel reinforcement details on deep-beam behavior subjected to shear loading.

$$F_2(x) = \left(\rho_v . f_{yv}\right)\left[1 - \frac{\rho_h . f_{yh}}{\rho_v . f_{yv} + \rho_h . f_{yh}}\right], x \in \Omega \quad (6)$$

Equation (7) establishes the relationship between concrete compressive strength (f_c')) and geometric efficiency, F_1 using the shear span ratio (a/d). The third performance index, F_3 includes concrete compressive strength (f_c') in the evaluation of shear performance. This index combines concrete strength (f_c') with geometric efficiency, F_1 (Equation (5)) using the shear span ratio (a/d), which controls the effectiveness of arching action in deep beams. The inclusion of the strength measure in the evaluation by multiplying it with the structural efficiency index, F_1 captures the effectiveness of concrete in contributing to shear resistance. The use of smaller shear spans improves the transfer of loads by compression struts, which in turn increases the effectiveness of concrete in the mechanism.

$$F_3(x) = \frac{f_c'}{a/d} F_1(x), x \in \Omega \quad (7)$$

Equation (8) represents the interaction of longitudinal reinforcement, geometry, and shear resistance deep beam. The F_4 represents the interaction of longitudinal tensile reinforcement and shear force demand on the member. It combines the influence of steel yield strength (f_y), geometric characteristics, and load intensity through the structural efficiency index. The presence of the shear span ratio (a/d) and section depth (d) indicates the influence of tensile forces in aiding the transfer of shear forces through internal stress redistribution. The coupling index embodies the joint influence of tension and shear forces that define deep beam response. The relationship between reinforcement characteristics and geometry and load factors combines to form a complete descriptor of the tensile-shear interaction.

$$F_4(x) = \rho . f_y . \frac{d}{a} . \frac{V}{h^2} F_1(x). , x \in \Omega \quad (8)$$

3.4 Rotational Multi-Objective Optimization (MOO)

Instead of attempting to solve a four-objective optimization problem simultaneously, this research work proposes four different multi-objective optimization (MOO) problems, each of which involves three objectives chosen from the complete list of performance measures (F_1, F_2, F_3, F_4). This rotational approach deliberately avoids one of the indices in each instance, which enables the research to examine the impact of the exclusion of a specific structural performance index on the optimal solutions obtained, as well as the sensitivity of the deep beam design problem to various combinations of objectives, as presented in Table 1.

Table 1: Four multi-objective optimization (MOO) cases with corresponding objective sets, excluded indices, and structural focus.

Case	Objective Set	Excluded Index	Remarks
MOO-1	F_1, F_2, F_3	F_4	Excludes tensile-shear coupling index; focuses on structural efficiency and reinforcement interactions
MOO-2	F_2, F_3, F_4	F_1	Excludes gross structural efficiency; emphasizes reinforcement and concrete utilization
MOO-3	F_1, F_2, F_4	F_3	Excludes tensile-shear coupling index; focuses on structural efficiency and reinforcement interactions
MOO-4	F_1, F_3, F_4	F_2	Excludes concrete utilization; highlights geometric efficiency and reinforcement interactions

Data-Driven Genome Bounding in Grasshopper

The experimentally derived bounds $x_i \in [x_i^{min}, x_i^{max}]$, obtained from the experimental database, were directly transferred into the parametric environment of Grasshopper to constrain the optimization variables at the source level. For each design variable, a corresponding slider was defined such that its admissible range exactly matched the limits extracted from the experimental data as shown by Equation (9).

$$Slider_i \in [x_i^{min}, x_i^{max}], i = 1, \dots, 13 \quad (9)$$

These sliders were then coupled directly to the Octopus genomes, such that each and every candidate vector produced during the course of the evolutionary search was automatically constrained by the experimental limits. This ensured that the optimizer was not allowed to venture into the non-physical regions of the solution space and that each and every solution produced

automatically satisfied the admissible domain condition ($x \in \Omega$). This ensured that the optimization process remained fully consistent with the experimentally observed deep beam behavior.

3.6 Data-Driven Genome Bounding in Grasshopper

For each identified MOO problem, the decision vector x and the objective functions (F_1, F_2, F_3, F_4) were directly connected to the Octopus evolutionary solver in Grasshopper. In this setup, the sliders used to represent the design variables are considered to be the genomes, and the performance indices are the fitness functions. The evolutionary solver evolves populations of candidate solutions based on Equation (10).

$$x^{(t+1)} = E(x^t) \tag{10}$$

where E denotes the evolutionary operators of selection, crossover, and mutation on the population in generation t. This continues for several generations until the difference in improvement between the fronts becomes insignificant, and a Pareto front is reached. A solution $x^* \in \Omega$ is said to be Pareto optimal if there is no other admissible solution that can improve one objective function without worsening at least one other objective function. This condition is adopted as per Equation (11).

$$\begin{bmatrix} F_1(x) \\ F_2(x) \\ F_3(x) \\ F_4(x) \end{bmatrix} \geq \begin{bmatrix} F_1(x^*) \\ F_2(x^*) \\ F_3(x^*) \\ F_4(x^*) \end{bmatrix}, x \in \Omega \tag{11}$$

with strict inequality satisfied for at least one component. This formulation in Equation (11) guarantees that the final set of solutions obtained by Octopus represents non-dominated deep-beam configurations that express optimal trade-offs among the chosen structural performance indices.

3.7 Pareto Front Extraction and Comparative Analysis

After the completion of the evolutionary search process, the Pareto fronts obtained from the four rotational MOO problems (Table 1) were extracted for further post-processing. As the Octopus solver returns "non-dominated" solutions, which are designs in which no single performance measure can be optimized without compromising another, these solutions indicate the theoretical optimum of structural performance in the specified range (Equation (3)). The comparison of the Pareto solutions is centered on the parametric changes induced by the objective prioritization. By cross-referencing the Pareto solutions, this analysis investigates how the physical system of the deep beam, particularly its geometric ratios (a/d), material quality (f_c'), and reinforcement layout, adjusts when the design priority is switched between efficiency (F_1) and structural gradient (F_4).

3. Results

3.1 MOO-1 (F_1, F_2, F_3)

The Pareto front of MOO-1 (Figure 2) shows clear structural patterns for 13 variables. F_1 (1.23-2305.18) distinguishes between compact and efficient designs and conservative shapes. F_2 (-2094.75

to 2560.25) represents a mechanical transition, where negative values indicate horizontal reinforcement dominance and positive values indicate vertical reinforcement control. F_4 (13.93-258183.15) represents the concrete strength and shear span-to-depth ratio interaction.

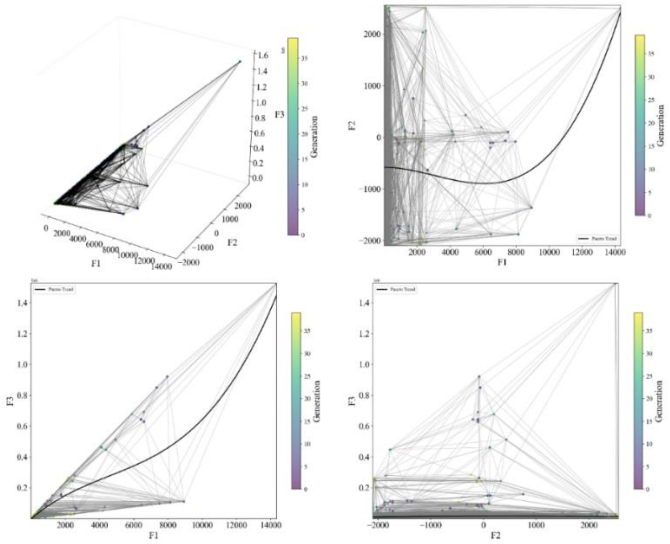

Figure 2: Pareto front visualization across 40 generations. The 3D plot shows solutions in F1, F2, and F3 space with Delaunay edges, while the 2D projections display each objective pair with nonlinear trend lines

The large numerical range of the indices verifies that the optimizer approached structurally different designs instead of converging to a set of nearby points. In the results post-processed in Figure 2, the progression of the multi-objective optimizer approaching an identifiable front, as denoted by the dark trendlines indicating an optimal balance of F_1, F_2, and F_3.

It is evident that the algorithm was successful in minimizing the objective conflict throughout the generational spectrum, moving from initial populations with higher dispersals to a denser, more populated front. This distribution of results again identifies an equilibrium among the deep beam designs in material economy and structural path requirements.

3.2 MOO-2 (F_2, F_3, F_4)

The MOO-2 Pareto front demonstrates varied structural approaches with a focus on internal mechanics. F_2 (–2094.75 to 2494.40) distinguishes between horizontal and vertical dominant reinforcement, pinpointing different shear transfer methods. F_3 (14 to 2.4×10^6) highlights the significant interaction between concrete strength and a/d ratios, with larger values indicating well-optimized concrete engagement. F_4 (0 to 22,000) indicates the tensile strength derived from longitudinal steel and geometric properties. The combined range of F_2, F_3 and F_4 validates that MOO-2 obtains distinct design approaches that balance material strength and reinforcement topological characteristics. Figure 3 clearly indicates a strong notion of convergence, as the progression from the scattered initial population to the refined frontier reinforces the optimizer's capacity to recognize complex internal mechanical trade-offs. The 2D projections clearly demonstrate non-linear trends within the Pareto optimal front for concrete usage (F_3) relative to tensile capacity (F_4), a fact that reinforces the notion of structural efficiency within optimized regions of non-linear fitted curve mobilization, with the high clustering towards the final frontier of the population output validates the definition of the generalized deep beam design paradigm as a function of the identified optimized synergistic relationship between reinforcement topology and concrete strength.

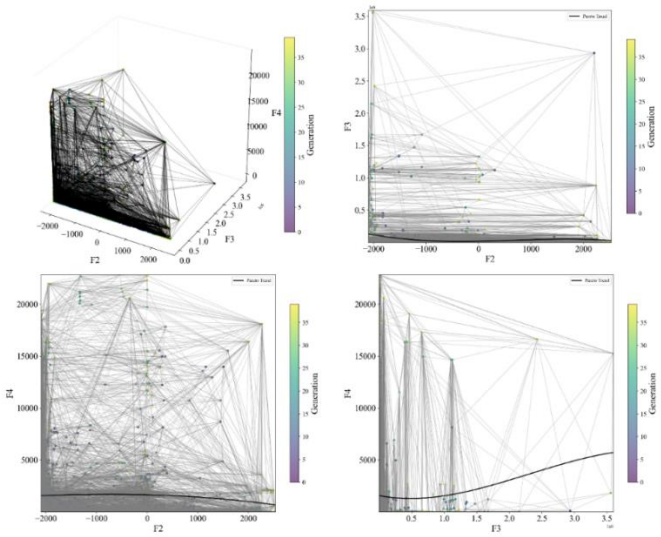

Figure 3: Pareto front visualization across 40 generations. The 3D plot shows solutions in F2, F3, and F4 space with Delaunay edges, while the 2D projections display each objective pair with nonlinear trend lines

3.3 MOO-3 (F_1, F_2, F_4)

The Pareto front of MOO-3 shows significantly different behavioral trends for three objectives. F_1 (0 to 2.2x10^4) tracks the point of transition from efficient to conservative designs. F_3 (0 to 6,500) reflects the balance of reinforcement, with larger values showing a dominant vertical reinforcement component in shear transfer. F_4 shows the largest variation (–2095 to +2540), which corresponds to varied tensile resistance designs, with capacity either limited by larger shear spans or increased by higher reinforcement ratios. This combined variation clearly supports the fact that MOO-3 formulates different geometric, reinforcement, and tensile designs, providing generalized design information rather than specific numerical answers.

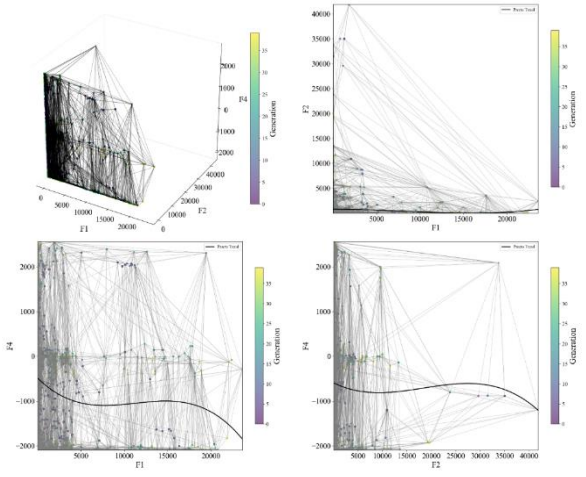

Figure 4 clearly demonstrates the complex and high-disperse convergence, as the transition from the initial stochastic populations to the final, more stabilized front highlights the optimization of non-linear design trade-offs.

https://doi.org/10.54878/xqyna996

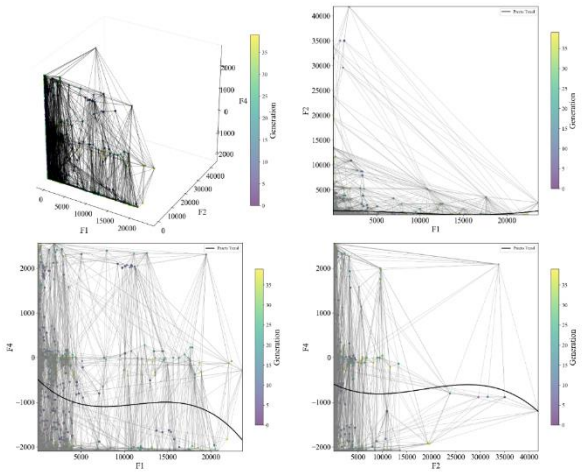

Figure 4: Pareto front visualization across 40 generations. The 3D plot shows solutions in F1, F2, and F4 space with Delaunay edges, while the 2D projections display each objective pair with nonlinear trend lines

The clearer 2D projection of the results demonstrates key behavioral boundaries, especially in the relationship between the F_1 and F_4 populations, as the parabolic trendline of the Pareto Set clearly defines the threshold between the mechanical properties of increased compactness in geometric designs and the augmentation of tensile capacities. The dense cluster of the final generation's solutions along the optimized front clearly demonstrates that the algorithm effectively maps the transition between diverse generalized deep beam behaviors

3.4 MOO-4 (F_1, F_3, F_4)

The Pareto front of MOO-4 shows a highly dispersed distribution, which indicates strongly varying design patterns. The function F_1 (0 to 2.2x10^4) clearly separates efficient designs from conservative ones, depending on their geometrical size. The function F_2 (14 to 2.4x10^6) shows a large dispersion in concrete use, where large values indicate the combined action of high-strength concrete and small shear span-to-depth ratios (a/d). The function F_3 (0 to 2.2x10^4) indicates strongly varying patterns of tensile resistance, which balance the amount of longitudinal reinforcement with geometrical constraints.

Figure 5 clearly illustrates the complex and high-disperse convergence of the multi-objective optimization process: it is evident that the transition from initial stochastic populations, visible as a light and scattered network, to the final, more stabilized front, represented by dense clusters, underlines the optimization of nonlinear design trade-offs. The parabolic trend line of the Pareto Set is well defined, especially in the projection of F_1 vs F_4. It clearly sets the threshold between mechanical properties of increased compactness in geometric designs and the augmentation of tensile capacities expressed by the maximization of steel utilization.

https://doi.org/10.54878/xqyna996

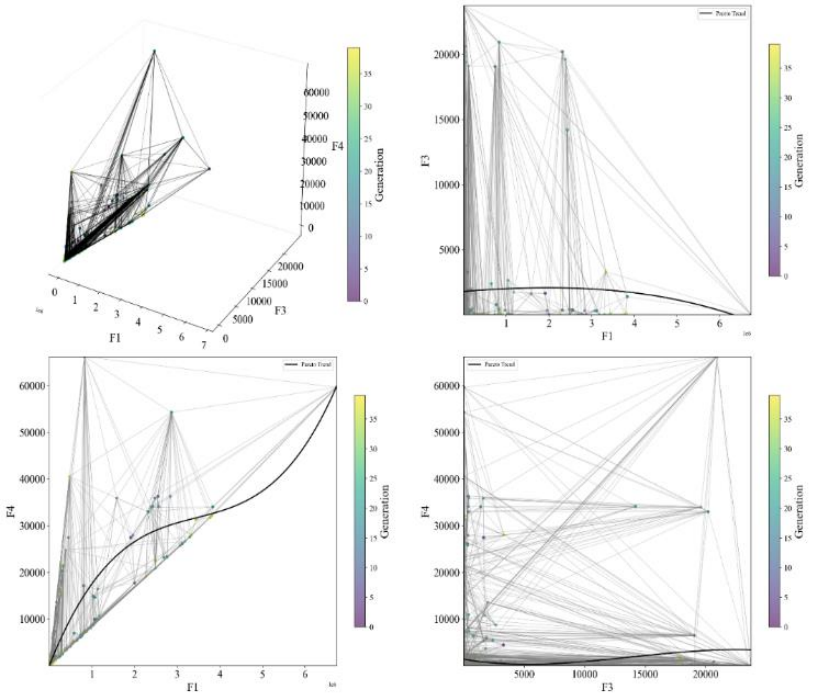

Figure 5: Pareto front visualization across 40 generations. The 3D plot shows solutions in F1, F3, and F4 space with Delaunay edges, while the 2D projections display each objective pair with nonlinear trend lines

4. Discussion

4.1 Geometric-Shear Demand Interaction

The performance measure F_1 expresses the relationship between sectional geometry and shear force requirements, correlating the cross-sectional area $(b.d)$ with the shear resistance (V). From all four Pareto solutions, the performance measure F_1 shows that deep beam performance is not dependent on absolute sectional size but rather on the geometric control of internal stress distributions for high shear transfer. The large spread of F_1 values confirms that for a given load, there exist multiple "optimal" geometries. The most efficient designs, with the lowest values of F_1, however, form a crucial point where the concrete volume is kept to a minimum without exceeding the material's ability to sustain a stable compression field. This suggests that the optimizer prioritizes the stress density of the strut-and-tie model than in expanding the beam volume.

The Pareto solutions show that quite different values of width (b) and depth (d) can lead to similar values of F_1. This is a clear indication that the load path in deep beams is determined by non-linear stress paths rather than linear flexural theories. Although an increase in depth (d) is beneficial in reducing the intensity of shear stress by increasing the size of the compression strut region, an increase in width (b) increases the cross-sectional area resisting the lateral force. Most importantly, the optimization solution shows a high degree of parametric interchangeability. A wider beam can offset a smaller depth and vice versa to achieve similar shear resistance patterns. This indicates that the optimization algorithm is not searching for a "golden ratio" of geometry, but rather a particular volumetric threshold that meets the equilibrium requirement of the internal strut-and-tie system. The Pareto fronts similarly demonstrate that these oversized sections aren't necessarily optimal because of the

principle of diminishing returns in the D-regions, in which any volume of concrete outside these core compression struts and tension ties is considered "dead weight" - less than optimal. The optimization similarly demonstrates that any increase in shearing force will simply result in a "geometric governor" in which the beam will be forced into a certain form that is most efficient in terms of allowance for efficient compression trajectories, rather than sheer volume. The focus is no longer simply on maximizing section size, but in finding the most streamlined form that will accommodate necessary stress trajectories without compressing the struts into a flat plane.

It should be noted that the Pareto approach exhibits the fact that deep beam geometry cannot be based on linear flexural stiffness design criteria applicable to slender beams, where efficiency is based on compatibility rather than internal shear stress flow. This optimization technique reinforces the basic principle that efficient design for a deep beam dictates compliance with its internal stress path, not necessarily the extremities of its dimensions. This method, therefore, introduces a paradigm shift towards a more efficient design approach where concrete usage is optimized and no longer based on conventional and conservative design practices.

4.2 Concrete Strength Utilization and Shear Span Effect

The objective F_2 regulates the equilibrium of vertical and horizontal reinforcement contributions in the deep beam region. In contrast to geometric objectives, F_2 emphasizes the mechanistic topology of the internal reinforcement, providing a quantitative assessment of the tensile load distribution in various directions. The objective F_2 plays a vital role in deep beam design, as the shear transfer mechanism, whether it is arch or truss action, is significantly dependent on the ratio of vertical stirrups to horizontal skin reinforcement. A higher value of F_2 represents a design with a predominance of vertical reinforcement, while a lower value represents a design where the horizontal reinforcement component is more prominent in resisting the splitting or sliding forces.

Analysis of the Pareto-optimal solutions for F_2 shows that for deep beams, there is considerable variation in the shear transfer approach based on the chosen reinforcement ratio. Solutions that result in higher values of F_2 are characterized by a design approach that emphasizes vertical stirrups to intercept diagonal cracks, which is a typical truss-like behavior. On the other hand, solutions with lower values of F_2 indicate a design approach that strategically emphasizes horizontal reinforcement, which is generally more effective in deep beams where the shear span-to-depth ratio is small and horizontal ties are required to resist splitting in the compression strut region. This is expected and confirms that the optimizer is not simply adding steel, but is looking for the most effective orientation-based resistance for a given load case.

The importance of reinforcement synergy in the mechanics of deep beams can be seen in the behavior represented by F_2. As D-regions, deep beams do not behave in the same manner as slender beams when it comes to load transfer. Rather, the development of a diagonal compression strut leads to a biaxial stress condition that requires stabilization by transverse steel reinforcement. The magnitude of this reinforcement interaction has a direct effect on the failure mode of the beam, either diagonal tension failure or sudden strut instability failure. F_2 behavior reveal the mobilization of material in either the vertical or horizontal direction. For example, there are several Pareto-optimal solutions that demonstrate balanced F_2 values, indicating optimal use of both reinforcement directions to stabilize the concrete strut.

In addition, F_2 captures the trade-off between vertical-dominant and horizontal-dominant reinforcement schemes. The designer has the flexibility to choose between a vertical stirrup arrangement that focuses on good confinement or a horizontal reinforcement ratio that enhances the arching action. The existence of multiple solutions in the Pareto set underlines the flexibility of the mechanistic approach in deep beam design, where the performance of the structure can be optimized together with construction details.

In the end, F_2 is essential in understanding the tensile efficiency of the deep beam section. This is because it enables the evaluation of the reinforcement used in relation to the stress trajectories. The optimization of F_2 ensures that the beam is capable of resisting the applied shear forces by either maximizing vertical dominance for crack control or horizontal dominance for strut stabilization. This is an essential goal in order to comprehend the mechanical properties of deep beams when they are subjected to shear forces.

4.3 Tensile Mechanism and Reinforcement Participation

The objective F_3 aims at evaluating the mechanism of tension as well as evaluating the actual contribution of the reinforcement in a structure of a deep beam, especially when loads are applied. Unlike slender beams, which mainly experience primary behavior, deep beams, as mentioned, exhibit the struts and tie model, in which the concrete will resist compression in the struts, while the tension will be resisted by the reinforcement. The efficient activation of the reinforcement is crucial for deep beams so that the progression of cracks is effectively checked. Optimizing F_3 helps in designing beams where the tensile reinforcement is neither underutilized nor overloaded.

Based on the analysis, tensile reinforcement participation sensitivity shows high sensitivity regarding the layout of the reinforcement, material properties, and loading conditions. Pareto optimal solutions indicate that beams with reinforcement aligned in the expected tension paths, especially those aligned in the principal tensile stress paths, have a uniform stress distribution and a delayed cracking moment. Conversely, a non-aligned reinforcement layout results in the localization of tensile stresses, which results in early cracking and a possible degradation in structural performance. This gives an idea of the importance of reinforcement alignment in the optimization of structural performance under certain conditions involving complex non-linear interactions between shear and bending effects.

The research also emphasizes the variation of the contribution of the reinforcement with the intensity of the load and the geometry of the beam. Beams with larger depth-to-span ratios (d/a) exhibit more pronounced effects of arching, which may result in a reduced direct load on the longitudinal reinforcement and an increased load on the transverse reinforcement in the tension zones. On the other hand, shallow deep beams depend more on the longitudinal tensile reinforcement to control the size of the cracks and provide stiffness to the structure. The participation factor, F_3 helps in determining the extent to which the reinforcement is actively working to resist the tensile forces rather than acting as redundant material.

As concrete tensile strength is surpassed, a change in equilibrium occurs around the reinforcement, an action for which F_4 seeks to optimize beam designs with the maximum steel activation and safety factor. Optimizing these designs indicate a fundamental balance between full activation and optimization of reinforcement and minimizing design and under-utilization potential; consequently, excellent serviceability is achieved by beam optimization regarding crack width and deformation curves. This approach directly compares with contemporary design

philosophies that view reinforcement as an exact science for improving durability and lifespan to beams and other structural constructs.

Ultimately, F_3 provides a comprehensive approach to achieving the maximum tensile system in deep beams. For one, the method will evaluate the engagement of the reinforcement with the applied load, highlight its link with concrete cracking, and ultimately lead to a better optimization of materials, all by concentrating on tensile participation in order to improve the overall role of reinforcement in structures, thus improving its role in safety and serviceability.

4.4 Integrated Structural Mechanism

The characteristics of the objective function F_4 relate to the optimization of deep beam performance; this is because, through such an optimization approach, numerous key design criteria can be synthesized. Unlike in other optimization techniques, which involve only a single criterion, it is apparent that deep beam performance is actually dependent on a group of variables, and the optimization of one particular mechanical property, such as the ratio of the reinforcement, influences the efficiency of the geometric mechanism of shear transfer.

As may be seen in analysis, the solutions may be Pareto optimal but are always located along a particular Pareto front, addressing simultaneously the most relevant trade-offs between the conflicting structural demands. Take, for example, structural configurations aiming to maximize load-carrying capacity by appropriately increasing the value of F_4, in contrast to, or in conjunction with, options aiming to minimize gross areas given by F_1. This captures the natural conflict in deep beam design, wherein the strut-and-tie modeling, tensile activation, and reinforcement mobilization need to be carefully integrated. Through the assessment of these trade-offs, Objective F_4 enables the selection of solutions that meet both high-performance and economic requirements.

The results also indicate that there are certain variables involved in design, which play a major role in the global performance index. The depth of the beam, longitudinal and shear reinforcement ratios, and shear span play a crucial role in maintaining the genetic diversity of all solution sets. The high genetic diversity of the solution set in the final generation ensures that the optimizer performs an extensive search of the design space, allowing for all possible structural responses, from slender to more conservative ductile members.

In summary, the results reveal that reinforcement layout proportional to expected stress path enhances the bearing capacity and the shear transfer at critical points with a high structural reliability and economic efficiency. With such an optimal design balance, the serviceability is ensured, which will reduce the crack width and increase the deflection profile, both contributing to prolonging the operational life of the structure. By holistically analyzing the mutual influence of geometry, material strength, and shear forces, the framework identifies Pareto-optimal solutions for complex deep beam configurations that traditional methods might overlook. Eventually, the employment of these objective functions creates a valuable strategy for both practical, project-specific optimization and the advancement of fundamental knowledge concerning deep beam behavior.

Conclusions:

This research confirms that multi-objective optimization offers the optimum approach for achieving high-performance deep beam designs. Some of the key findings can be listed as follows:

i. The Pareto Optimal method is capable of achieving fine balances between all of the competing requirements involving load carrying capacity, deflection, and crack

control, thus producing cost-efficient and economical design solutions.

ii. Further, the effective engagement of reinforcement with respect to the principal stress trajectories is a major aspect; i.e., its alignment directly impacts the load-carrying capacity and amount of cracking.

iii. Structural optimality is attained not by over-using, but by intelligent usage of reinforcement, thus proving that topology is as important as volume of the material being employed.

iv. Beam depth, strength, and reinforcement are the most significant factors in determining the structural behavior, which allows for the optimization of the performance with the use of minimal materials.

Recommendations:

Recommendations on the basis of these findings are presented for the design and detailing of deep beams based on the results of this multi-objective analysis:

i. Structural designers need to look beyond single objective-based capacity evaluations and consider multi-objectives. This would indeed provide well-rounded performance in terms of ultimate strength, serviceability in terms of deflection and crack resistance, and economic viability, among others, and would fill the gap between theoretical approaches and actual construction.

ii. Hence, there is a need to appropriately address the detailing of reinforcement with due emphasis on areas experiencing high tensile stress, following a concept that is in accordance with Strut-and-Tie Modeling (STM). It is to be noted that alignment of steel reinforcement intended to guide the principal directions of tensile stress is of more value than reinforcing simply with a higher volume.

iii. The designer must apply optimization techniques to arrive at minimum percentages required in the minimum ratios of effective reinforcement. Thus, there will be no possibility for over-reinforcing this section due to human error, as it will result in unnecessary cost expenditure without optimally enhancing safety levels proportionally.

iv. It should be noted that the depth of the beam, concrete strength, and reinforcement ratio cannot be individually examined; instead, designers should conduct a sensitivity analysis to optimize these factors as their interaction directly influences the efficiency of the compression zone and safety margin of the D-region.

Acknowledgements

This research was conducted independently and was not funded.

Declarations

Funding

This research received no external funding.

Competing Interests

The author(s) declare that they have no known competing financial or non-financial interests that could have appeared to influence the work reported in this paper.

Ethics Approval

This study did not involve human participants, human data, or animal subjects. Therefore, ethical approval was not required.

Author Contributions

Tufail Mabood: Conceptualization, methodology, software development, validation, writing, data curation, formal analysis, writing original draft.

Data Availability Statement

Data and optimization scripts are available at: [https://github.com/tufailmab/DeepBeam-MOO-Optimization]. Requests for additional data may be directed to the corresponding

author. (Note: Repository will be set to public upon publication).

Generative AI Declaration

No AI was used.

References

P. Salehi, R. Aghayari, and M. Fazelikelareh, "Behavioral Analysis of Reinforced Concrete Deep Beams under Dynamic Loading with Varying Strain Rates Using the Strut-and-Tie Model Framework," Civil Engineering Infrastructures Journal, Nov. 2025, doi: 10.22059/CEIJ.2025.398909.2350.

M. R. Kaloop et al., "Shear Strength Estimation of Reinforced Concrete Deep Beams Using a Novel Hybrid Metaheuristic Optimized SVR Models," Sustainability (Switzerland), vol. 14, no. 9, May 2022, doi: 10.3390/su14095238.

F. Cakir and M. A. Ozdemir, "Strut-and-Tie Modeling of Intraply Hybrid Composite-Strengthened Deep RC Beams," Buildings 2025, Vol. 15, Page 3810, vol. 15, no. 21, p. 3810, Oct. 2025, doi: 10.3390/buildings15213810.

H. Chen, Y. Sun, and M. Deng, "Research on the Reinforcement Design of Concrete Deep Beams with Openings Based on the Strut-and-Tie Model," Buildings 2025, Vol. 15, Page 1382, vol. 15, no. 8, p. 1382, Apr. 2025, doi: 10.3390/buildings15081382.

W. A. Jasim, A. A. Allawi, and N. K. Oukaili, "Strength and Serviceability of Reinforced Concrete Deep Beams with Large Web Openings Created in Shear Spans," Civil Engineering Journal, vol. 4, no. 11, pp. 2560-2574, Nov. 2018, doi: 10.28991/cej-03091181.

M. Mansour and T. El-Maaddawy, "Testing and modeling of deep beams strengthened with NSM-CFRP reinforcement around cutouts," Case Studies in Construction Materials, vol. 15, no. 3, pp. 145-152, Dec. 2021, doi: 10.1016/j.cscm.2021.e00670.

A. Al-khreisat, M. Abdel-Jaber, and A. Ashteyat, "Shear Strengthening and Repairing of Reinforced Concrete Deep Beams Damaged by Heat Using NSM-CFRP Ropes," Fibers, vol. 11, no. 4, Apr. 2023, doi: 10.3390/fib11040035.

A. Al Ismaeel, F. Amin, and A. Husnain, "Predicting the shear strength of RC deep beams with wide openings using FEM and machine learning-based Ni-Ti SMA retrofitting," Results in Engineering, vol. 29, no. 6, p. 109320, Mar. 2026, doi: 10.1016/j.rineng.2026.109320.

Q. Hussain and A. Pimanmas, "Shear strengthening of RC deep beams with openings using Sprayed Glass Fiber Reinforced Polymer Composites (SGFRP) : Part 1. Experimental study," KSCE Journal of Civil Engineering, vol. 19, no. 7, pp. 2121-2133, Feb. 2015, doi: 10.1007/s12205-015-0243-1.

J. M. Mhalhal, T. S. Al-Gasham, and S. R. Abid, "Tests on reinforced concrete deep beams with different web reinforcement types," IOP Conf. Ser. Mater. Sci. Eng., vol. 988, no. 1, Dec. 2020, doi: 10.1088/1757-899X/988/1/012032.

C. Ma, S. Wang, J. Zhao, X. Xiao, C. Xie, and X. Feng, "Prediction of shear strength of RC deep beams based on interpretable machine learning," Constr. Build. Mater., vol. 387, Jul. 2023, doi: 10.1016/j.conbuildmat.2023.131640.

A. Tiwari, A. K. Gupta, and T. Gupta, "A robust approach to shear strength prediction of reinforced concrete deep beams using ensemble learning with SHAP interpretability," Soft Comput., vol. 28, no. 7-8, pp. 6343-6365, Apr. 2023, doi: 10.1007/s00500-023-09495-w.

K. Le Nguyen, H. Thi Trinh, T. T. Nguyen, and H. D. Nguyen, "Comparative study on the performance of different machine learning techniques to predict the shear strength of RC deep beams: Model selection and industry implications," Expert Syst. Appl., vol. 230, Nov. 2023, doi: 10.1016/j.eswa.2023.120649.

D. C. Feng, W. J. Wang, S. Mangalathu, G. Hu, and T. Wu, "Implementing ensemble learning methods to predict the shear strength of RC deep beams with/without web

reinforcements," Eng. Struct., vol. 235, May 2021, doi: 10.1016/j.engstruct.2021.111979.

H. Chen, W. J. Yi, and H. J. Hwang, "Cracking strut-and-tie model for shear strength evaluation of reinforced concrete deep beams," Eng. Struct., vol. 163, pp. 396-408, May 2018, doi: 10.1016/j.engstruct.2018.02.077.

M. M. Hameed, F. Khaleel, M. K. AlOmar, S. F. Mohd Razali, and M. A. Alsaadi, "Optimising the selection of input variables to increase the predicting accuracy of shear strength for deep beams," Complexity, vol. 2022, 2022, doi: 10.1155/2022/6532763.

M. Shahnewaz, A. Rteil, and M. S. Alam, "Shear strength of reinforced concrete deep beams—A review with improved model by genetic algorithm and reliability analysis," Structures, vol. 23, pp. 494-508, Feb. 2020, doi: 10.1016/j.istruc.2019.09.006.

A. F. Ashour, L. F. Alvarez, and V. V. Toropov, "Empirical modelling of shear strength of RC deep beams by genetic programming," Comput. Struct., vol. 81, no. 5, pp. 331-338, Mar. 2003, doi: 10.1016/S0045-7949(02)00437-6.

M. V. G. Silveira, L. A. G. Bitencourt, and S. Das, "Generative design framework for RC deep beams using topology optimization and generative tie method: Experimental and numerical investigation," Eng. Struct., vol. 316, p. 118490, Oct. 2024, doi: 10.1016/j.engstruct.2024.118490.

"(PDF) APPLICATION OF TOPOLOGY OPTIMIZATION ON DEEP BEAMS." Accessed: Feb. 05, 2026. [Online]. Available: https://www.researchgate.net/publication/360943746_APPLICATION_OF_TOPOLOGY_OPTIMIZATION_ON_DEEP_BEAMS

Q. F. Hasan, D. A. Al-Mamany, and O. K. Fayadh, "Design of Reinforced Concrete Deep Beams using Particle Swarm Optimization Technique," Karbala International Journal of Modern Science, vol. 5, no. 4, pp. 254-265, 2019, doi: 10.33640/2405-609X.1180.

H.-Z. Zhang, Z.-S. Wu, X.-X. Yuan, and W.-T. Xu, "Performance of Deep Beams with Topologically Optimized Reinforcements: Experimental Verification and Comparison," Journal of Structural Engineering, vol. 151, no. 4, p. 04025019, Apr. 2025, doi: 10.1061/jsendh.steng-13495.

H. Wang, C. Zhang, and H. Wu, "Shear Capacity Prediction Model of Deep Beam Based on New Hybrid Intelligent Algorithm," Buildings 2023, Vol. 13, Page 1395, vol. 13, no. 6, p. 1395, May 2023, doi: 10.3390/buildings13061395.

E. H. Houssein, M. Hossam Abdel Gafar, N. Fawzy, and A. Y. Sayed, "Recent metaheuristic algorithms for solving some civil engineering optimization problems," Scientific Reports 2025 15:1, vol. 15, no. 1, pp. 7929-, Mar. 2025, doi: 10.1038/s41598-025-90000-8.